

**BEZIER-LIKE FUNCTIONS FOR
CONSTRUCTING CRANIOFACIAL FRACTURES**

ABDUL MAJEED

UNIVERSITI SAINS MALAYSIA

2016

**BEZIER-LIKE FUNCTIONS FOR
CONSTRUCTING CRANIOFACIAL FRACTURES**

by

ABDUL MAJEED

**Thesis submitted in fulfilment of the requirements
for the degree of
Doctor of Philosophy**

September 2016

ACKNOWLEDGEMENT

I thank Almighty ALLAH who give me strength for the successful completion of my research.

I would like to express my deepest gratitude to my supervisor Professor Dr. Abd Rahni Mt Piah of Universiti Sains Malaysia, for all his guidance, support, patience, advice, suggestions and above all give me free hand to work which enable me to write this thesis and complete my Ph. D work, for which I am extremely grateful.

My special honour also goes to Universiti Sains Malaysia, especially to the Dean of the School of Mathematical Sciences and the Ministry of Higher Education of Malaysia for giving me an opportunity to study and providing me with the facilities and financial assistance to pursue my higher degree. I would like to thanks my field supervisors Professor Dr. Malik Zawwaar Hussain and Associate Professor Dr. R.U Gobithaasan for their kind help and support and would like to give my appreciation to my brothers, Major M Rafique and Dr Hassan Iqbal for their kind help in proof-reading my thesis.

Last but certainly not least, I would like to express my love and appreciation to my parents and my wife for their understanding and great support at all the time and to all my other family members and friends who had either directly or indirectly help me to complete my study.

TABLE OF CONTENTS

Acknowledgement	ii
Table of Contents	iii
List of Tables	vii
List of Figures	viii
List of Abbreviations	xvi
Abstrak	xvii
Abstract	xix

CHAPTER 1 – INTRODUCTION

1.1	Introduction	1
1.2	Research Problem	3
1.3	Objectives	4
1.4	Significance Of Study	5
1.5	Thesis Overview	5

CHAPTER 2 – BACK-GROUND AND LITERATURE REVIEW

2.1	Anatomy of Craniofacial Region	7
2.2	Causes of Craniofacial Fracture	7
2.3	Craniofacial Fracture Diagnosis	8
2.3.1	X-rays	8
2.3.2	CT-Scan	9
2.4	Data Used in Thesis	10
2.5	Literature Review	13
2.6	Summary	15

CHAPTER 3 – BEZIER-LIKE FUNCTIONS

3.1	Basis Functions	16
3.1.1	Ball Curve	19
3.1.2	Effect of Control Points and Shape Parameters	20
3.1.3	Parametric and Geometric Continuity	22
3.2	The Rational Cubic Ball Curves	24
3.2.1	C^1 Rational Cubic Ball Curves	25
3.2.2	Tangent Vectors	26
3.2.3	GC^1 and GC^2 Rational Cubic Ball Curves	26
3.3	B-Spline Basis Functions	28
3.3.1	The B-spline Curves	31
3.4	The Non Uniform Rational B-Spline (NURBS) Curves	37
3.5	Summary	41

CHAPTER 4 – SURFACE CONSTRUCTION

4.1	Bi-cubic Rational Ball Surface	42
4.2	Surface By Contour Blending Method	44
4.3	Summary	46

CHAPTER 5 – MATHEMATICAL FOUNDATION

5.1	Boundary Extraction	47
5.1.1	Mathematical Morphology	47
5.2	Corner Detection	49
5.2.1	First Pass	50
5.2.2	Second Pass	51
5.2.3	Parameters	52
5.2.4	Demonstration	52
5.3	Parameterization	53

5.4	Least Square Method	56
5.5	Normalized Mean Squares Error	59
5.6	Genetic Algorithm	59
5.6.1	Search Space	60
5.6.2	Initial Population	60
5.6.3	Natural Selection	61
5.6.4	Pairing	61
5.6.5	Crossover	62
5.6.6	Mutations	63
5.6.7	Example	63
5.6.8	The Next Generations	68
5.6.9	Demonstration	70
5.7	Curve to DICOM Format	72
5.8	Graphical User Interface GUI	73
5.9	Summary	74

CHAPTER 6 – RESULTS AND ANALYSIS

6.1	Construction of Craniofacial Fractures in 2D Form	75
6.2	Construction of Fracture Parts in 3D Form	90
6.3	Comparative Analysis	96
6.4	Validity of Proposed Methods	104
6.4.1	Quantitative Analysis	104
6.4.2	Qualitative Analysis	106

CHAPTER 7 – CONCLUSION

REFERENCES	117
-------------------	------------

LIST OF PUBLICATIONS

LIST OF TABLES

		Page
Table 5.1	Example initial population of 8 random chromosomes and their corresponding cost	64
Table 5.2	Surviving chromosomes after a 50% selection rate	65
Table 5.3	Pairing and mating process of single point crossover chromosome family binary string cost	65
Table 5.4	Mutating the population	67
Table 5.5	New ranked population at the start of the second generation	68
Table 5.6	Population after crossover and mutation in the second generation	69
Table 5.7	New ranked population at the start of the third generation	69
Table 5.8	Ranking of generation 3 from least to most cost	70
Table 6.1	Slice 188 errors	105
Table 6.2	Slice 195 errors	106

LIST OF FIGURES

	Page
Figure 1.1 Craniofacial bones (taken form Gray et al. (1973))	3
Figure 2.1 X-ray machine. (HUSM)	8
Figure 2.2 CT-scan machine. (HUSM)	9
Figure 2.3 CT scan images of patient with frontal bone fracture	10
Figure 2.4 CT scan images of patient with right side parietal bone fracture	11
Figure 2.5 CT scan images of patient with left side parietal bone fracture	11
Figure 2.6 CT scan images of patient with occipital bone fracture	12
Figure 2.7 CT scan images of patient with multiple bone fracture	12
Figure 3.1 Ball basis functions ($n = 2$)	17
Figure 3.2 Bezier basis functions ($n = 3$)	17
Figure 3.3 Timmer basis functions ($n = 4$)	18
Figure 3.4 Variation diminishing property with $b = 1, p = 3, k = 1$	20
Figure 3.5 Effect of P_1 (control point)	21
Figure 3.6 Effect of P_2 (control point)	21
Figure 3.7 Effect of shape parameter a_1	22
Figure 3.8 Parametric continuity	23
Figure 3.8(a) C^0 continuity $P(1) = Q(0)$	23
Figure 3.8(b) C^1 continuity $P^i(1) = Q^i(0), i = 0, 1$	23
Figure 3.8(c) C^2 continuity $P^i(1) = Q^i(0), i = 0, 1, 2$	23

Figure 3.9	Geometric continuity	24
Figure 3.9(a)	GC^1 continuity $\lambda = 1.3$	24
Figure 3.9(b)	GC^2 continuity $\lambda = 0.5, \gamma = 1.2$	24
Figure 3.10	Uniform B-spline basis functions	30
Figure 3.10(a)	$n = 0$	30
Figure 3.10(b)	$n = 1$	30
Figure 3.10(c)	$n = 2$	30
Figure 3.10(d)	$n = 3$	30
Figure 3.11	Non uniform cubic B-spline basis ($n = 3$)	31
Figure 3.12	Boundary of CT scan image	36
Figure 3.13	B-spline curve fitting with 10 knots	36
Figure 3.14	B-spline curve fitting with 17 knots	37
Figure 3.15	B-spline curve fitting with 20 knots	37
Figure 5.1	Boundary of vase	48
Figure 5.1(a)	Vase image	48
Figure 5.1(b)	Binary image	48
Figure 5.1(c)	Vase boundary	48
Figure 5.2	Boundary of 'Dal'	48
Figure 5.2(a)	'Dal' image	48
Figure 5.2(b)	Binary image	48
Figure 5.2(c)	'Dal' boundary	48
Figure 5.3	Boundary of CT scan image	49
Figure 5.3(a)	CT scan image	49
Figure 5.3(b)	Binary image	49
Figure 5.3(c)	Boundary of CT scan image	49

Figure 5.4	The contour point P_j at maximum perpendicular distance from the straight line P_iP_k .	51
Figure 5.5	Superfluous candidate corner point P_j in (a) and (c).	52
Figure 5.6	Corner points for vase	53
Figure 5.6(a)	Vase image	53
Figure 5.6(b)	Boundary of vase	53
Figure 5.6(c)	Boundary with corner points	53
Figure 5.7	Corner points for CT scan image	53
Figure 5.7(a)	CT scan image	53
Figure 5.7(b)	Boundary of CT scan image	53
Figure 5.7(c)	Corner points	53
Figure 5.8	Chord length parameterization	55
Figure 5.9	A uniformly spaced vs chord length parameterization	56
Figure 5.10	Vase reconstruction	71
Figure 5.10(a)	Vase boundary	71
Figure 5.10(b)	Reconstructed boundary using rational Ball curve	71
Figure 5.11	Reconstruction of Bear	71
Figure 5.11(a)	Bear image	71
Figure 5.11(b)	Reconstructed image using rational Ball curve	71
Figure 5.12	Reconstructed boundary of CT scan	72
Figure 5.12(a)	Bear image	72
Figure 5.12(b)	Reconstructed image using rational Ball curve	72
Figure 5.13	Curve to DICOM format	73
Figure 6.1	Boundary extraction for different CT scan images	76
Figure 6.1(a)	Image	76

Figure 6.1(b)	Boundary of image (a)	76
Figure 6.1(c)	Image	76
Figure 6.1(d)	Boundary of image (c)	76
Figure 6.1(e)	Image	76
Figure 6.1(f)	Boundary of image(e)	76
Figure 6.2	Reconstructed boundary curves of complete slice	77
Figure 6.2(a)	Reconstructed boundary curve using C^1 rational cubic Ball curves	77
Figure 6.2(b)	Reconstructed boundary curve using GC^1 rational cubic Ball curves	77
Figure 6.2(c)	Reconstructed boundary curve using GC^2 rational cubic Ball curves	77
Figure 6.2(d)	Reconstructed boundary curve using B-spline curves	77
Figure 6.2(e)	Reconstructed boundary curve using NURBS curves	77
Figure 6.3	Construction of frontal bone fractured part curves using C^1 rational cubic Ball curves	78
Figure 6.3(a)	Original image of frontal bone fracture	78
Figure 6.3(b)	Boundary of image (a)	78
Figure 6.3(c)	Construction of fracture part curves	78
Figure 6.4	Construction of frontal bone fractured part in DICOM format	79
Figure 6.5	Construction of parietal bone fractured part curves using GC^1 rational cubic Ball curves	79
Figure 6.5(a)	Original image of parietal bone fracture	79
Figure 6.5(b)	Boundary of parietal bone fracture	79
Figure 6.5(c)	Parietal bone fractured part curves construction	79
Figure 6.6	Construction of parietal bone fractured part curves for different CT scan slice using GC^1 rational cubic Ball curves	80
Figure 6.7	Effect of shape parameters	81
Figure 6.7(a)	inner $a = 2.123$, $b = 2.39$, $\lambda = 2.10$, outer $a = 2.012$, $b = 2.10$, $\lambda = 6.12$	81

Figure 6.7(b)	inner $a = 2.10$, $b = 2.23$, $\lambda = 2.04$, outer $a = 2.02$, $b = 2.09$, $\lambda = 6.12$	81
Figure 6.7(c)	inner $a = 2.10$, $b = 2.12$, $\lambda = 2.004$, outer $a = 2.04$, $b = 2.029$, $\lambda = 6.001$	81
Figure 6.7(d)	inner $a = 2.076$, $b = 2.10$, $\lambda = 2.001$, outer $a = 2.004$, $b = 2.012$, $\lambda = 6$	81
Figure 6.7(e)	inner $a = 2.0199$, $b = 2.010$, $\lambda = 1.99$, outer $a = 2.001$, $b = 2.0012$, $\lambda = 5.99$	81
Figure 6.8	Construction of parietal bone fracture part in DICOM format	82
Figure 6.9	Construction of parietal bone fracture part in DICOM format for different CT scan slices	82
Figure 6.10	Construction of parietal bone fractured part curves for different CT scan slices using GC^2 rational cubic Ball curves	83
Figure 6.11	Construction of parietal bone fractured part in DICOM format for different CT scan slices using GC^2 rational cubic Ball curves	83
Figure 6.12	Construction of parietal bone fractured part curves for different CT scan slices using B-spline curves	84
Figure 6.13	Construction of parietal bone fractured part in DICOM format for different CT scan slices using B-spline curves	85
Figure 6.14	Construction of multiple bone fracture part curves for different CT scan slices using NURBS curves	85
Figure 6.15	Construction of multiple bone fracture part in DICOM format for different CT scan slices using NURBS curves	86
Figure 6.16	Skull bone thickness of different CT scan slices	86
Figure 6.17	Skull bone thickness of different position	87
Figure 6.18	Thickness of reconstructed fracture part	87
Figure 6.19	GUI using GC^1 rational cubic Ball curves	88

Figure 6.20	GUI using GC^2 rational cubic Ball curves	89
Figure 6.21	GUI using B-spline curves	89
Figure 6.22	CT scan data with frontal bone fracture in 3D form	91
Figure 6.23	Fractured part curves in 3D form	91
Figure 6.24	Construction of fractured part intermediate curves in 3D form	92
Figure 6.25	Front view of constructed frontal bone fracture part in 3D form using bi-cubic rational Ball function	92
Figure 6.26	Inner view of constructed frontal bone fracture part in 3D form using bi-cubic rational Ball function	93
Figure 6.27	Construction of frontal bone fractured part in 3D form using contour blending method	93
Figure 6.28	CT scan data in 3D format	94
Figure 6.29	The front view of reconstructed 3D craniofacial fracture using contour blending method	95
Figure 6.30	The side view of reconstructed 3D craniofacial fracture using contour blending method	95
Figure 6.31	CT scan image of slice 188	96
Figure 6.32	Construction of fractured part curve using C^1 rational Ball curves	97
Figure 6.33	CT scan image of slice 170	97
Figure 6.34	Construction of fractured part curve using C^1 rational Ball curves	98
Figure 6.35	Construction of fractured part curve using GC^1 rational Ball curves	98
Figure 6.36	Comparison of C^1 , GC^1 rational Ball curves	99
Figure 6.37	CT scan slice with big fractured part	100
Figure 6.38	Construction of fractured part curve using GC^1 rational Ball curves with one segments	100

Figure 6.39	Construction of fractured part curve using GC^1 rational Ball curves with three segments	101
Figure 6.40	Construction of fractured part curve using GC^2 rational Ball curves with three segments	101
Figure 6.41	Construction of fractured part curve using B-spline curves with three segments	102
Figure 6.42	Effect of control points on B-spline curve	103
Figure 6.43	Construction of fractured part curve using NURBS curve with three segments	103
Figure 6.44	Reconstruction of complete CT scan slice 188 boundary curves	105
Figure 6.44(a)	Boundary	105
Figure 6.44(b)	Reconstructed boundary curve using GC^1 rational cubic Ball curves	105
Figure 6.45	Reconstruction of complete CT scan slice 195 boundary curves	106
Figure 6.45(a)	Boundary	106
Figure 6.45(b)	Reconstructed boundary curve using B-spline curves	106
Figure 6.46	Reconstruction of complete skull boundary curves	107
Figure 6.46(a)	Original image	107
Figure 6.46(b)	Boundary	107
Figure 6.46(c)	Reconstructed boundary curves using GC^1 rational Ball curves	107
Figure 6.47	Reconstruction of complete skull in DICOM format	107
Figure 6.48	Pre-operation CT scanned images of patient	108
Figure 6.49	CT scanned images of patient with occipital bone fracture	109
Figure 6.50	Post-operation (inserted skull) CT scanned images of patient	109
Figure 6.51	Construction of fractured part curves for different post-operation (inserted skull) CT scanned images	110

Figure 6.52	Fractured part in DICOM format of post-operation CT scanned image	111
Figure 6.53	Fractured part in DICOM format for different post-operation CT scanned images	111
Figure 6.54	Reconstruction of boundary curves	112
Figure 6.54(a)	Original image	112
Figure 6.54(b)	Image supposed to be fractured	112
Figure 6.54(c)	Reconstructed boundary curves using GC^1 rational Ball curves	112
Figure 6.55	Reconstruction of fractured part in DICOM format	113
Figure 6.55(a)	Original image	113
Figure 6.55(b)	Fractured part in DICOM format	113
Figure 6.55(c)	Combine image	113
Figure 6.56	Reconstruction of boundary curves	113
Figure 6.56(a)	Original image	113
Figure 6.56(b)	Image supposed to be fractured	113
Figure 6.56(c)	Reconstructed boundary curves using B-spline curves	113
Figure 6.57	Reconstruction of fractured part in DICOM format	114
Figure 6.57(a)	Original image	114
Figure 6.57(b)	Fractured part in DICOM format	114
Figure 6.57(c)	Combine image	114

LIST OF ABBREVIATIONS

GA	Genetic Algorithm
CT	Computerized Tomography
MRI	Magnetic Resonance Imaging
DICOM	Digital Imaging and Communications in Medicine
GUI	Graphical User Interface
CAD	Computer Aided Design
CAM	Computer Aided Manufacturing
HUSM	Hospital Universiti Sains Malaysia
NURBS	Non-Uniform Rational B-Spline
SAM06	Sarfraz Asim Masood 06

FUNGSI BAK-BEZIER UNTUK MEMBENTUK KRANIOFASIAL YANG RETAK

ABSTRAK

Kecacatan kraniofasial atau kecederaan sekunder daripada trauma adalah satu cabaran sekunder untuk mendiagnos dan merawat, kedua-duanya bagi seorang pakar radiolo-gi dan pakar bedah yang merawat kerana kedudukan anatomi kompleks dalam tubuh manusia. Pembinaan bahagian retak kraniofasial membolehkan penyelidik yang ber-minat mencadangkan suatu model defek atau kecacatan dan memudahkan doktor yang merawat untuk menyediakan protokol pengurusan yang sebaik mungkin kepada pesa-kit. Dalam kepustakaan, teknik yang berbeza seperti menggunakan pencerminan, mo-del rujukan dan teknologi Reka Bentuk Berbantuan Komputer (CAD) / Reka Bentuk Berbantuan Pembuatan (CAM) digunakan untuk pembinaan keretakan kraniofasial. Tesis ini mencadangkan pembinaan bahagian yang hilang pada keretakan kraniofasial dengan menggunakan lengkung nisbah bak-Bezier dengan keselantaran yang berbe-za seperti C^1 , C^2 , GC^1 dan GC^2 . Keselantaran peringkat yang lebih tinggi bermakna kelicinan yang lebih baik pada lokasi pertemuan sepunya antara lengkung tembereng bersebelahan. Penyesuaian lengkung sepunya dicapai menggunakan kaedah kuasa dua terkecil untuk mengoptimumkan titik kawalan pertengahan dan parameter bebas di-kira menggunakan algoritma genetik (GA). Dalam mengesahkan kaedah yang dica-dangkan, imej 2D pelbagai objek seperti beruang, pasu dan huruf Arab 'Dal' dibina. Kaedah yang dicadangkan digunakan untuk membina semula lengkung sempadan su-

atu tengkorak penuh. Morfologi matematik digunakan untuk menentukan sempadan tengkorak yang dipilih. Lengkung dalam dan luar bahagian yang retak dibina dalam bentuk format 2D diimbas iaitu Tomografi Berkomputer (CT), dalam bentuk Imej Digital dan Komunikasi dalam Perubatan (DICOM). Bahagian yang dibina kemudiannya ditukar kembali kepada format DICOM. Akhirnya, keputusan yang diperolehi daripada kaedah ini menggunakan beberapa fungsi bak-Bezier dibandingkan di antara satu sama lain. Untuk menjadikan pembinaan berguna dan mesra pengguna kepada seorang doktor yang merawat atau pakar bedah, satu antara muka pengguna grafik (GUI) telah dibangunkan. Tujuan GUI ini ialah untuk meminimumkan prosedur dan masa bagi membantu seorang doktor atau pakar bedah merawat pesakitnya yang mengalami keretakan kraniofasial tanpa perlu memahami algoritma atau matematik di sebalik pembinaannya. Untuk membina kraniofasial 3D yang retak, kontur 2D ditukar kepada bentuk 3D dengan membentuk bersama komponen-z sama jarak yang sepadan. Kemudian, satu kaedah adunan kontur dan fungsi nisbah bi-kubik bak Bezier digunakan untuk membina bahagian yang retak dalam 3D. Kaedah yang dicadangkan dalam tesis ini adalah berdasarkan data DICOM sahaja dan tidak memerlukan mana-mana teknik lain seperti pengimejan cermin atau tengkorak rujukan. Dengan menggunakan kaedah yang dicadangkan, implan retak yang dibina adalah buatan tersesuai bagi seseorang pesakit. Dalam tesis ini, data imbasan CT daripada lima kes sebenar keretakan kraniofasial diperolehi daripada Hospital Universiti Sains Malaysia (HUSM) untuk menguji kesesuaian dan keberkesanan kaedah yang dicadangkan dalam situasi sebenar.

BEZIER-LIKE FUNCTIONS FOR CONSTRUCTING CRANIOFACIAL FRACTURES

ABSTRACT

Craniofacial deformity or injury secondary to trauma is a challenge to diagnose and treat, both for a radiologist and a treating surgeon due to its complex anatomical location in the human body. The construction of craniofacial fracture parts enables an interested researcher to propose a model of the defect or deformity and to facilitate the treating physician in providing the best possible management protocol to his/her patient. In the literature, different techniques such as using mirroring, reference model and Computer Aided Design (CAD) / Computer Aided Manufacturing (CAM) technology are employed for a construction of craniofacial fractures. This thesis proposes a construction of missing parts of craniofacial fracture using Bezier-like rational curves with different continuities namely C^1 , C^2 , GC^1 and GC^2 . Higher order continuity means smoother common joint between adjacent curve segments. Curve fitting is achieved using the least squares method to optimize intermediate control points and free parameters are calculated using Genetic Algorithm (GA). In order to validate the proposed method, 2D images of various objects such as a bear, a vase and an Arabic letter '*Dal*' are constructed. The proposed method is applied to reconstruct the boundary curve of a full slice. Mathematical morphology is used to determine the boundary of the chosen skull. Inner and outer curves of a fractured part are constructed in 2D form of the Computed Tomography (CT) scanned data which are in Digital Imaging

and Communications in Medicine (DICOM) format and in 2D format, respectively. The constructed parts are then converted back to DICOM format. Finally, results obtained from this method using several Bezier-like functions are compared to each other. For the construction to be useful and user-friendly to a treating doctor or a surgeon, a Graphical User Interface (GUI) has also been developed. The aim of this GUI is to minimize the procedure and the time to help this doctor or surgeon treating his/her patient with craniofacial fracture without having to understand the algorithm or mathematics behind its construction. To construct the 3D craniofacial fracture, a 2D contour is converted to a 3D form by forming together corresponding equidistant z -components. Then, a contour blending method and bi-cubic rational Bezier-like functions are applied in order to construct the fractured part in 3D. The proposed method used in this thesis is based on DICOM data only and does not require any other technique such as mirror imaging or reference skull and there is no need to take the average thickness of skull bone. Using the proposed method, the constructed fractured implant is custom-made for any patient. In this thesis, CT scanned data for five real cases of craniofacial fractures are obtained from the Hospital Universiti Sains Malaysia (HUSM) to test the methods applicability in real life situation.

CHAPTER 1

INTRODUCTION

1.1 Introduction

With the advent of modern technologies in various fields and technology oriented business environment, the use of computers has become a basic need. To implement the algorithms and 3D designing of various products, computer aided geometric design (CAGD) has played a vital role. CAGD is also called geometric modelling, refers to the research stream for the development and representation of different forms of free form curves and surfaces.

The concept of CAGD emerged in 1970s and expanded in various fields such as automotive industry, aerospace and rapid prototype machines. Barnhill and Riesenfeld introduced this field in a conference in which they discussed different aspects of CAGD at University of Utah, USA in 1974. After this conference, the field evolved in a systematic manner with enhanced features and insights in different technological aspects. In this context, the first formal book on this topic appeared with the title "Computational Geometry for Design and Manufacturing" authored by Faux and Pratt (1979) that was based on the previous fundamental work of Coons (1964).

There is an exponential growth in the development of CAGD due to advancement in processing techniques, advanced mathematical models and computations of complex problems. Irrespective the type of scientific field such as automobile, aircraft, aerospace, ship industries and pharmaceutical industries, CAGD has been embedded in the core processes. CAGD was first developed for hard core technology such as

automobiles and aeronautical to implement the complicated designs of various components and assemblies. However, since last decade, CAGD has become a mature technology and is being used in various technologies especially having complicated designs including bio-modelling. This work takes into account application of CAGD in bio-modelling and specifically focuses on the construction of craniofacial fracture by using Bezier-like functions.

Craniofacial region of human body is a complex region. It is made of various bones integrated together in a complex fashion. Fractures of craniofacial region can occur due to trauma, falls and sports injury. Figure 1.1 shows various bones that make up this region. Different diagnostic imaging tools are being used to diagnose fractures of craniofacial region like X rays, CT scan and Magnetic Resonance Imaging (MRI).

The aim of reconstruction of craniofacial region is to achieve and restore both the esthetics and normal physiological function. As explained earlier, craniofacial region is a complex anatomical location and disruption in the bony continuity of this region is detrimental to both esthetics and functionality. It is always challenging to diagnose fractures of the craniofacial region. Most of the times, clinical examination is insufficient and requires radiological imaging tools to diagnose these fractures.

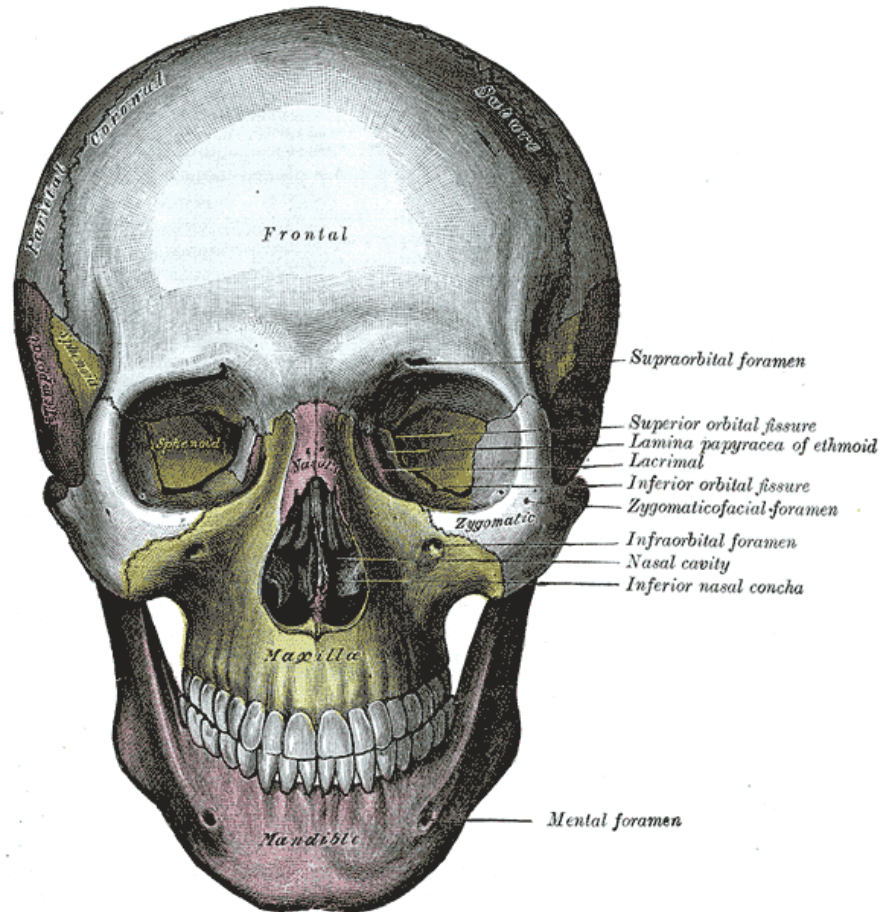


Figure 1.1: Craniofacial bones (taken from Gray et al. (1973))

1.2 Research Problem

This study is an attempt to provide the best possible technique for the reconstruction of craniofacial fracture by using Bezier-like basis functions. This research work will provide the method independent of reference model, mirror imaging, statistical model, external help in the form of technician and to take the average thickness of constructed bone. We will be able to attain required thickness of bone through this proposed method. Moreover, this study will add to the existing literature by presenting the technique which furnishes the custom made implant for every individual patient and reduces the chances of infection, gives faster recovery to patients. For this, dif-

ferent possible curves like Ball curve with different continuities between two curve segments, B-spline curves and NURBS curves have been applied. The proposed technique requires only CT scan data of patient for fracture reconstruction.

Clinical cases are also included in this thesis to show the important application of the proposed methods. Matlab has been used to develop a Graphics User Interface (GUI) for craniofacial reconstruction using the proposed methods, which can be used by surgeons without in-depth understanding of its mathematical knowledge. The CT scan data are obtained from Hospital Universiti Sains Malaysia (HUSM).

1.3 Objectives

This thesis aims to achieve the following objectives:

- To provide an alternative method for the construction of craniofacial fractures using Bezier-like basis functions.
- To develop a graphical user interface for the construction of fractured part curves for those without or limited knowledge in mathematics.
- To provide the method which preserves the required thickness of constructed bone.
- To provide the methods for the construction of fractured part into 3D form.
- To provide the initial platform of custom-made implant for every patient with craniofacial fractures.

1.4 Significance Of Study

This study is significant because

- This study will provide the methods to attain the required thickness of bone.
- This study will provide the custom made implant for every unique patient.
- This study will provide the best solution or treatment option for the benefit of the patient.
- This study will reduce morbidity, mortality and hospital cost.

1.5 Thesis Overview

Chapter 1 provides a background of CAGD and overview of the contributions for different researchers. The objective and significance of study is also discussed in this chapter. Chapter 2 explains the anatomy of craniofacial region, the causes of craniofacial fractures and how to diagnose the fracture. The real data of five different patient are also discussed in this chapter.

The Bezier-like functions along with properties, Ball curves, effect of control points and shape parameters and parametric and geometric continuity condition are explained in Chapter 3. The construction of cubic rational Ball curves with C^1 , GC^1 and GC^2 continuities, B-spline basis functions, the cubic B-spline curves and NURBS curves are also discussed in this chapter. Chapter 4 explains two different methods, bi-cubic rational Ball surface and surface by contour blending for the construction of craniofacial fracture in 3D form.

To extract the boundary of each CT scan image, mathematical morphology will be used

and the Sarfraz Asim Mahmood 2006 (SAM06) method as in Sarfraz (2008) will be used to obtain the corner points. The least squares method will be used to optimize the intermediate control points, normalized least square method will be used as a cost function in genetic algorithm (GA) and GA will be used to optimize the shape parameters of proposed methods. All these methods are explained in Chapter 5. The method for the construction of fractured part from curve to DICOM format and construction of GUI are also explained in this chapter.

Chapter 6 gives the implementation of proposed methods and consists of four sections. Section one explains construction of fracture part curves using proposed methods explained in Chapter 3. The construction of fracture part in DICOM format is also explained in this section. The construction of 3D craniofacial fractures using proposed methods are explained in section two. The comparative analysis of proposed methods is explained in section three. The validity of proposed method is explained in last section of Chapter 6. Chapter 7 concludes the thesis.

CHAPTER 2

BACK-GROUND AND LITERATURE REVIEW

This chapter discusses the anatomy of craniofacial fracture, its causes and ways to diagnose it. Real craniofacial data of five different patients are also discussed in this chapter. The last section of this chapter explains the literature review.

2.1 Anatomy of Craniofacial Region

Craniofacial region is a complex anatomical location in the human body and fracture to craniofacial region does not follow a classic pattern. A number of small bones join together to form craniofacial region adding to its complexity, thus, leading to difficulty in diagnosing and treating the fractures Gray et al. (1973). The bones of the craniofacial region include bones around the eyes (orbital bones), cheekbone (zygoma), cranial bones (the top portion of the skull that protects the brain), frontal bone, lower jaw (mandible), nasal bone, upper jaw (maxilla) and parietal bone as shown in Figure 1.1.

2.2 Causes of Craniofacial Fracture

Common etiological factors of the craniofacial fractures include sports-related injuries, gunshot trauma, motor vehicle accidents and some time due to internal injury and brain tumor. Craniofacial fractures range from mild to severe.

2.3 Craniofacial Fracture Diagnosis

Apart from clinical expertise, sophisticated radiological imaging is required to help in the diagnosis of craniofacial fractures. The spectrum of radiological imaging stretch from plain X-ray films to CT scan and MRI.

2.3.1 X-rays

Various different angulation of the beam are required to get a plain X-rays in the diagnosis of craniofacial fractures like submentovertex X-rays is obtained when zygomatic bone, particularly, the zygomatic arch fractures are suspected. To diagnose the mandibular condylar fractures, reverse Towns view is taken. Figure 2.1 represents the image of X-ray machine.



Figure 2.1: X-ray machine. (HUSM)

2.3.2 CT-Scan

Although various types of X-ray views may help to diagnose craniofacial fractures but even then majority of the fractures require more sophisticated imaging. Since the invention of CT scans, compound to complex craniofacial fractures are mostly diagnosed using the CT scans (Righi et al., 2015). CT scans are good to project the bony contours of the anatomical location. Recently, the reconstruction of CT scan films to three dimension and intraoperative use of CT scan has opened new avenues (Shaye et al., 2015). The fractures site is reconstructed to 3D that makes it easier for both the radiologists and surgeons to diagnose and treat the fractures. Figure 2.2 represents the image of CT scan machine (HUSM) which is used to obtain the CT scan data for the current work.



Figure 2.2: CT-scan machine. (HUSM)

2.4 Data Used in Thesis

To construct the craniofacial fracture, radiological data of five different patients with frontal bone, multiple bone, occipital bone and parietal bone fractures will be used in this thesis. Figure 2.3 represents the CT scan images of patient with frontal bone fracture. Figure 2.4 represents the CT scan images of patient with right side parietal bone fracture. The patient with parietal bone fracture on left side is represented in Figure 2.5. The CT scan images of patient with occipital bone fracture are represented in Figure 2.6. The CT scan images of patient with multiple bone fracture are represented in Figure 2.7.

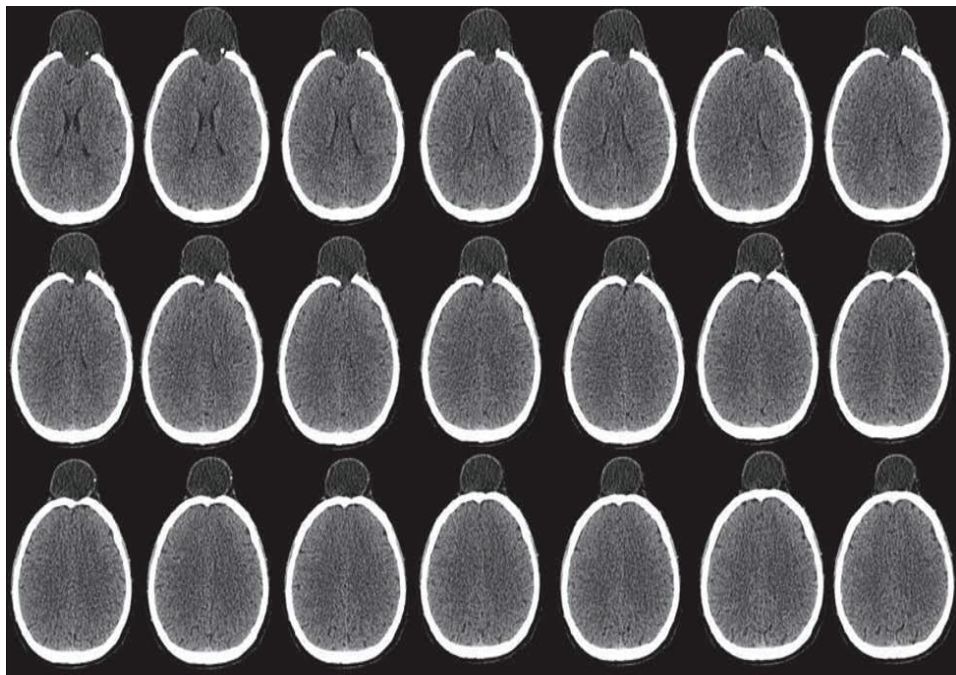


Figure 2.3: CT scan images of patient with frontal bone fracture

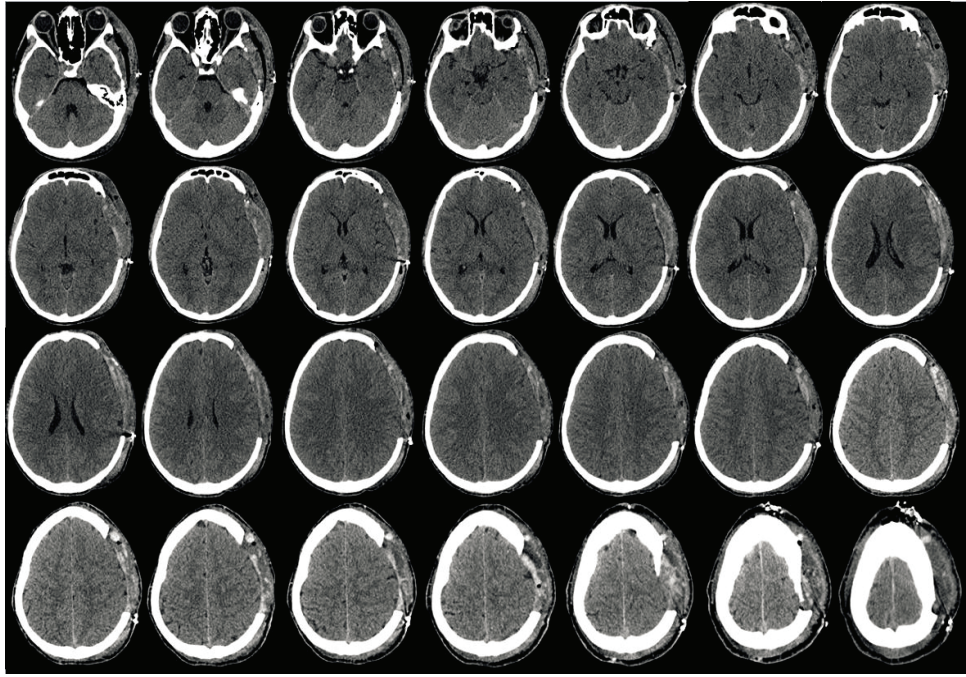


Figure 2.4: CT scan images of patient with right side parietal bone fracture

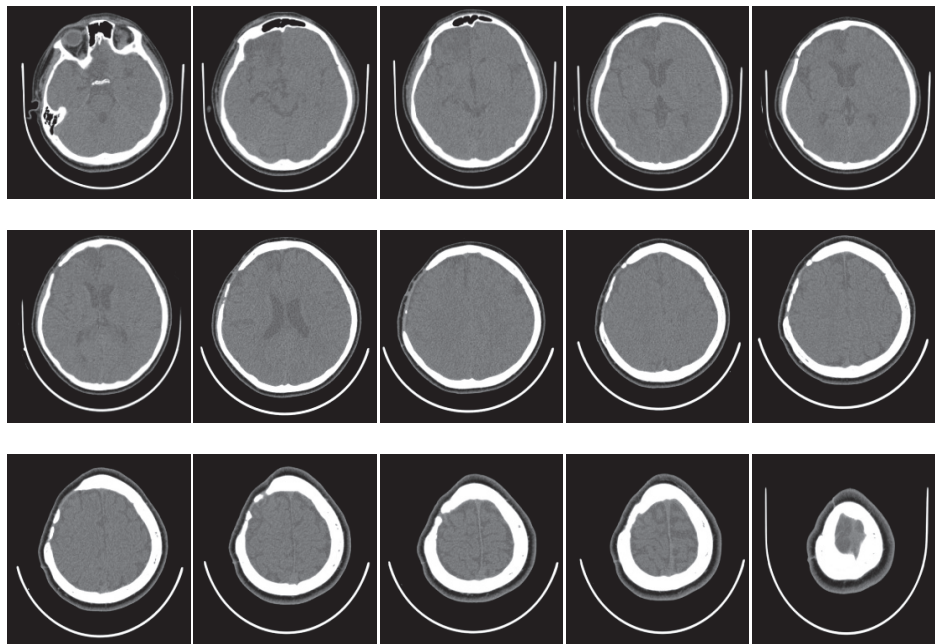


Figure 2.5: CT scan images of patient with left side parietal bone fracture

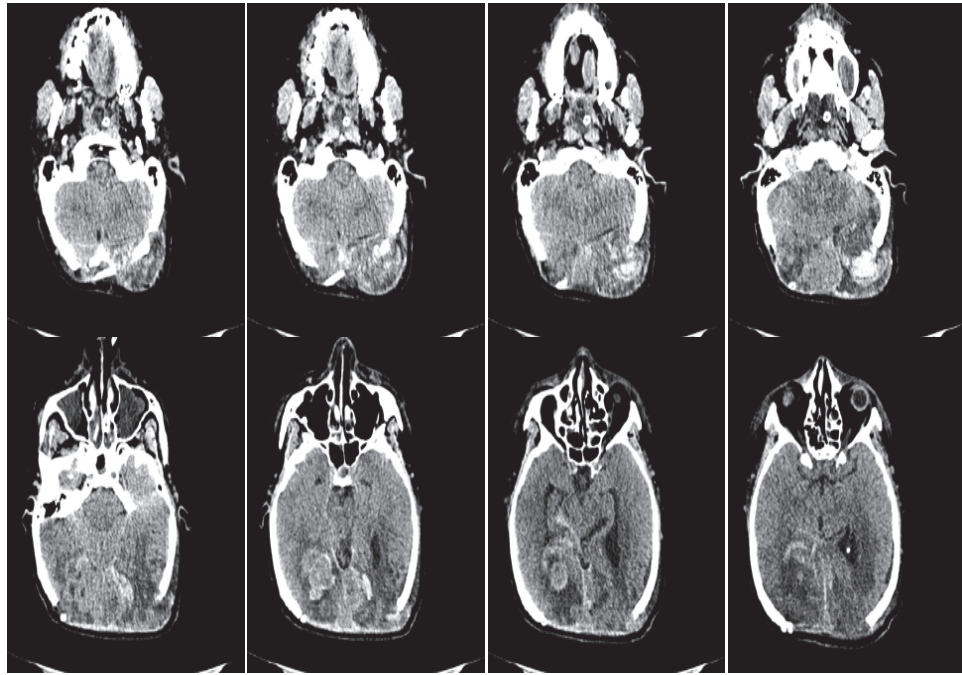


Figure 2.6: CT scan images of patient with occipital bone fracture

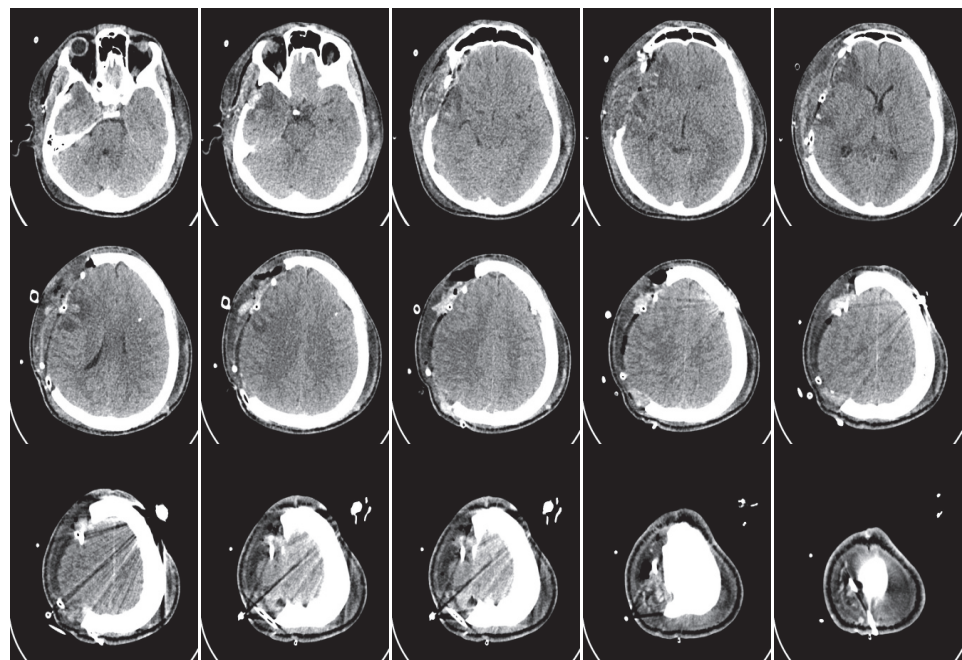


Figure 2.7: CT scan images of patient with multiple bone fracture

2.5 Literature Review

The advent of computer vision technology has opened new frontiers for mathematicians, engineers and doctors to help in the diagnosis and reconstruction of the craniofacial defects caused by tumors and trauma. The craniofacial fracture reconstruction work started in early nineties. Different researchers used different methods for fracture reconstruction. Eufinger et al. (1995) and Müller et al. (2003) used CAD/CAM process for the craniofacial reconstruction. In this approach, technical staff and tools are required to help surgeons, which causes low efficiency, high cost and the construction of large format fracture becomes difficult using CAD/CAM.

Sauret et al. (2002) proposed mirroring method and Min and Dean (2003) used deformation or surface interpolation. These methods use either mathematical or anatomical features for craniofacial fracture reconstruction. The mirroring method is useful for the fracture on one side of the skull only and it uses anatomical features while mathematical constraints are used in interpolation and deformation methods to construct the fractured part from the non-fractured part of the skull. Adaptive deformation method for reconstruction of the fracture is proposed by Wu et al. (2006) and Wuyang et al. (2010). In this method, the authors had first constructed reference model according to patient's skull and then performed a 3D matching for the correlation between reference skull and patient skull. This proposed technique is applied to construct the fractured region of skull corresponding to reference skull.

To reproduce the 2D manual reconstruction, Miyasaka et al. (1995) proposed a computer imaging system. In order to maintain and guarantee the accuracy, they build 20 parts data base involving eyes, nose, contours and hairstyle. Soft tissue thickness technique is proposed by Lee et al. (1999), though this proposed method is tedious, time

consuming and requires the help of anatomical and artistic expertise.

Archer (1997) and Archer et al. (1998) have used hierarchical B-spline interpolation. They have elaborated the landmarks to reconstruct the facial region by the computer technology. Kang (2006) and Shui et al. (2010) used 37 landmarks to construct craniofacial fractures. Facial reconstruction is dependent on the registration of dense points. The base of facial reconstruction method is to distort the reference skull to unknown skull based on correspondence landmarks and then use these deforms on reference skull to get craniofacial fracture reconstruction. Suetens et al. (2006) used Thin Plate Spline (TPS) to reconstruct the craniofacial fracture taking 52 landmarks. Turner et al. (2005) adopted Iterative Closest Point (ICP) taking into account 30 skull model database.

Claes et al. (2006) presented Principal Component Analysis (PCA) to generate statistical model to build the guide skull and face model. Finally, Thin Plate Spline (TPS) was used to convert the guide to unidentified skull to reconstruct the fractured part. Desvignes et al. (2006) constructed a statistical craniofacial model between face and skull, after this, one can estimate the appearance of unidentified skull directly. Zhang et al. (2010) proposed a regional statistical craniofacial model to enhance the accuracy of craniofacial fracture reconstruction.

The craniofacial fracture reconstruction, of unknown skull, along with outlook evaluation from one template, generation of statistical model and organs integration based on Chinese people involving four steps is proposed by Wuyang et al. (2010).

Lee et al. (2002) proposed a rapid prototyping model to produce custom made implant for the reconstruction of large cranial defect. Berar et al. (2005) suggested a technique to construct a 3D statistical model of face and skull. To reconstruct the cranium de-

fault, Heissler et al. (1998) proposed a custom made titanium implants generated with CAD/CAM. The detail of present computer based craniofacial method is explained by Claes et al. (2010). The tissue map based fracture reconstruction method is proposed by Pei et al. (2008).

Liang et al. (2009) proposed the method for the construction of fracture based on Chinese people. Kähler et al. (2001) reconstructed the realistic muscle components attached on the skeletons. Carr et al. (1997) had constructed the cranial defect using radial basis functions (RBF) in which they took the average thickness of bone. For more related work (see Quatrehomme et al. (2007), Berar et al. (2011), Claes et al. (2010), Pei et al. (2008), Tu et al. (2007), Vandermeulen et al. (2006), Bhatt and Warkhedkar (2008), de Aquino et al. (2011), Stephan (2003), Wilkinson (2004), Wilkinson and Neave (2003), Carr et al. (1997), and references therein)

2.6 Summary

The anatomy of craniofacial fracture, causes and how to diagnose the craniofacial fracture have been explained in this chapter. The real CT scan data for five different patients used in this work has also been explained in Section 2.5. This chapter has also included the literature review.

CHAPTER 3

BEZIER-LIKE FUNCTIONS

Bezier form is one of the most well known mathematical representation of curves and surfaces being used in computer aided design and computer graphics. Two Frenchmen; Pierre Bezier at Renault and Paul de Casteljaou at Citroen introduced Bezier curve while working in automobile industry during the period of 1958 – 60. Abhyankar and Bajaj (1987) and Forrest (1972) further developed the Bezier curves.

In this chapter, section one explains the Bezier-like cubic basis functions. Parametric and geometric continuity between two curve segments are also discussed in this section. Rational cubic Ball curves with different continuity conditions are explained in section two. Section three explains B-spline basis functions and curves. Last section pertains to the NURBS functions and curves.

3.1 Basis Functions

The Bezier like cubic basis functions $S_i(\theta), i = 0, \dots, 3$ are defined in Ali (1994) as:

$$\begin{aligned} S_0(\theta) &= (1 - \theta)^2(1 + (2 - n)\theta), \quad S_1(\theta) = n\theta(1 - \theta)^2, \\ S_2(\theta) &= n\theta^2(1 - \theta), \quad S_3(\theta) = \theta^2(1 + (2 - n)(1 - \theta)). \end{aligned} \tag{3.1}$$

Where n is a positive integer. For $n = 2$ the functions become cubic Ball basis functions defined by Ball (1974) and Said (1989). Figure 3.1 represents the graphical behavior of Ball basis functions. The functions become cubic Bezier basis if $n = 3$ as defined by

Farin et al. (2002). The graphical behavior of cubic Bezier basis is shown in Figure 3.2.

If $n = 4$, functions are called the cubic Timmer basis as defined by Timmer (1980) and shown in Figure 3.3. In this thesis, Ball basis functions will be used for the construction of craniofacial fractures.

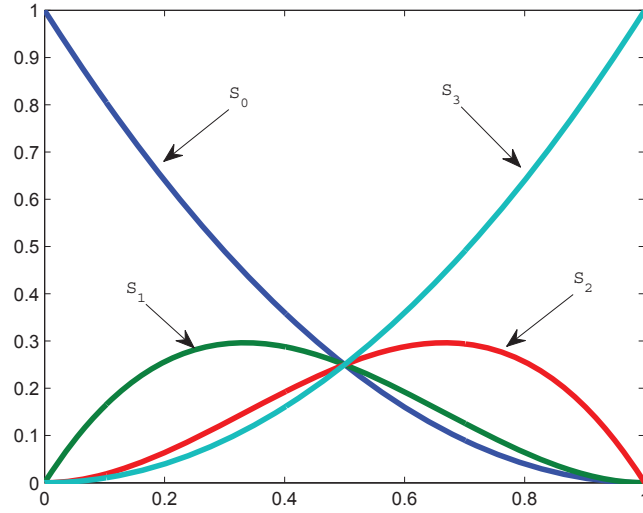


Figure 3.1: Ball basis functions ($n = 2$)

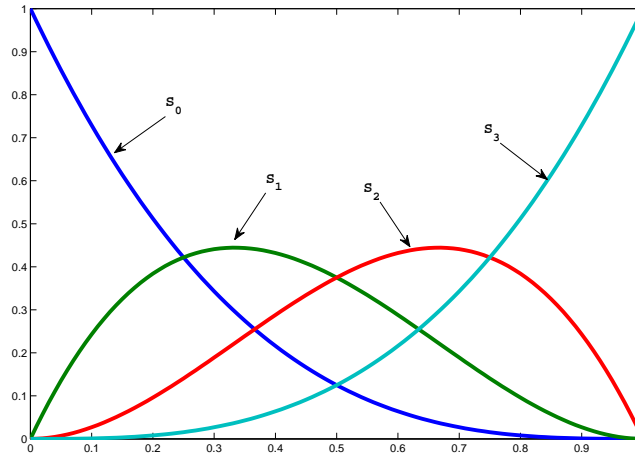


Figure 3.2: Bezier basis functions ($n = 3$)

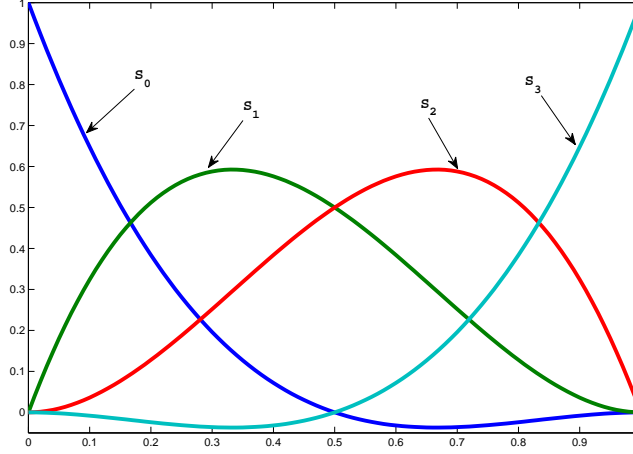


Figure 3.3: Timmer basis functions ($n = 4$)

The Ball basis functions defined in Equation (3.1) have the following properties:

- **Linearly Independent:** The Ball basis functions are linearly independent. There do not exist as set of non zero constants a_0, \dots, a_3 , for which

$$\sum_{i=0}^3 a_i S_i(\theta) = 0.$$

- **Non-Negative:** Ball basis functions are non-negative when $\theta \in [0, 1]$.
- **Symmetric:** The Ball basis functions are symmetric as

$$S_i(\theta) = S_{3-i}(1 - \theta).$$

- **Monotonicity:** $S_0(\theta)$ is monotonically decreasing and $S_3(\theta)$ is monotonically increasing when $\theta \in [0, 1]$.
- **Partition of Unity:** Ball basis functions form a partition of unity, it means that sum of Ball basis functions is always 1.

$$\sum_{i=0}^3 S_i(\theta) = 1.$$

3.1.1 Ball Curve

If P_i be the set of control points and $S_i(\theta)$, $i = 0, \dots, 3$ be Ball basis functions as defined in Equation (3.1), then Ball curve $s(\theta) = \sum_{i=0}^3 P_i S_i(\theta)$ has the following properties:

- **Coordinate system independence:** As the Ball basis functions form partition of unity, the Ball basis curve will be independent of coordinate system. It means that by changing the coordinate system of control points, the curve will remain the same.
- **Convex Hull Property:** The Ball curve obeys the coordinate system independence and Ball basis functions are all non negative. Therefore, Ball curves will obey the convex hull property. This means that curves formed by Ball basis always lie within the convex hull of their control points.

$$\sum_{i=0}^3 S_i(\theta) = 1, \quad S_i(\theta) \geq 0, \quad 0 \leq \theta \leq 1, \quad i = 0, \dots, 3.$$

- **Variation Diminishing Property (VDP):** Variation Dimension Property is obeyed by Ball curve. VDP is stated as: if a curve is intercepted by straight line in b , number of points and control polygon by p number of points, then it will always hold that

$$b = p - 2k$$

as shown in Figure 3.4, where k is 0 or a positive integer.

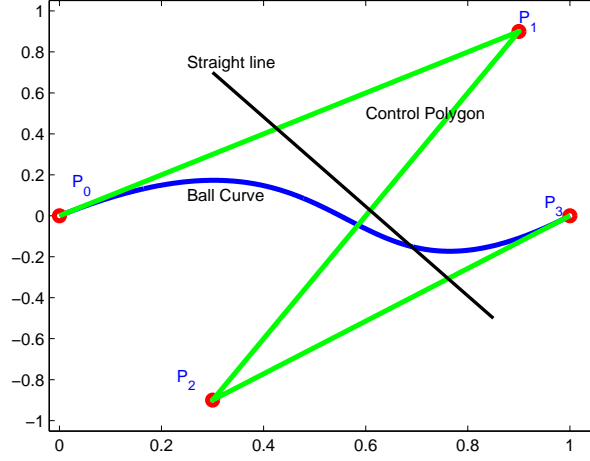


Figure 3.4: Variation diminishing property with $b = 1$, $p = 3$, $k = 1$

3.1.2 Effect of Control Points and Shape Parameters

Let $P_i \in \mathbb{R}^2$ be the set of control points, a_i be non-negative shape parameters and $S_i(\theta)$, $i = 0, \dots, 3$ be Ball basis functions. The Ball curve $s(\theta) = \sum_{i=0}^3 P_i a_i S_i(\theta)$ can be changed or controlled by twofold. Firstly, by intermediate control points. By changing the position of control point P_1 the curve bends towards P_1 as shown in Figure 3.5. Similarly by changing the position of control point P_2 the curve bends towards P_2 as shown in Figure 3.6.

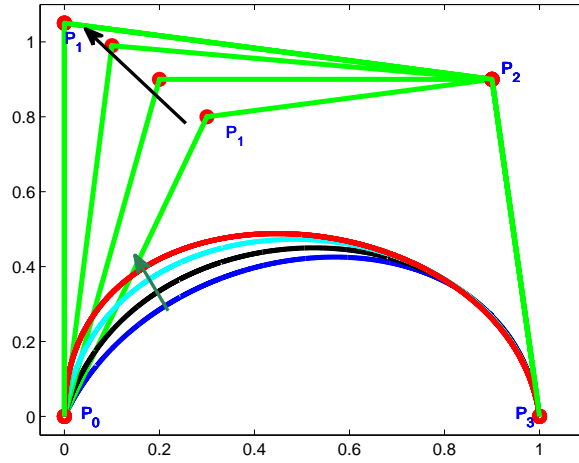


Figure 3.5: Effect of P_1 (control point)

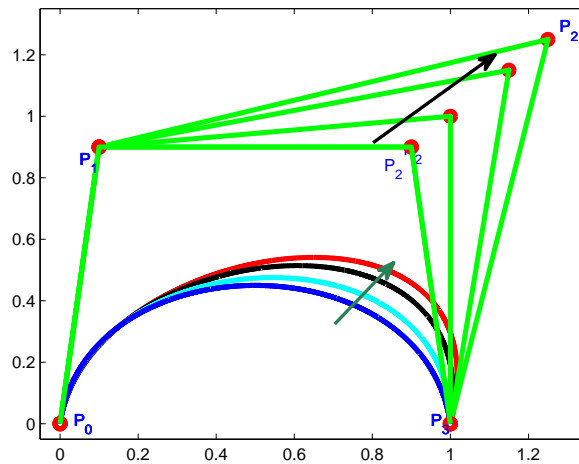


Figure 3.6: Effect of P_2 (control point)

Secondly, by changing the shape parameters. For example in Figure 3.7, the curve bends towards P_1 by changing the value of a_1 .

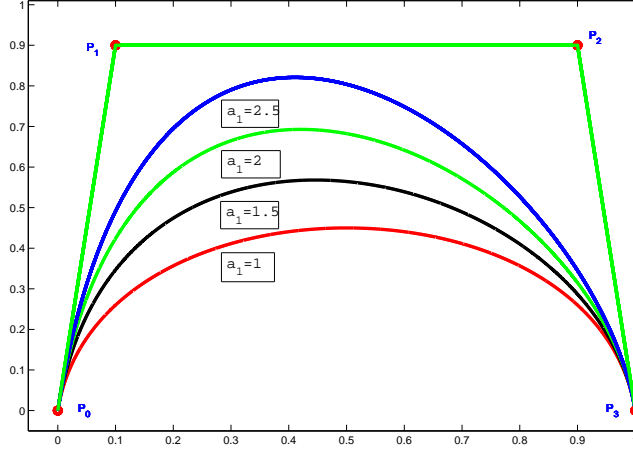


Figure 3.7: Effect of shape parameter a_1

3.1.3 Parametric and Geometric Continuity

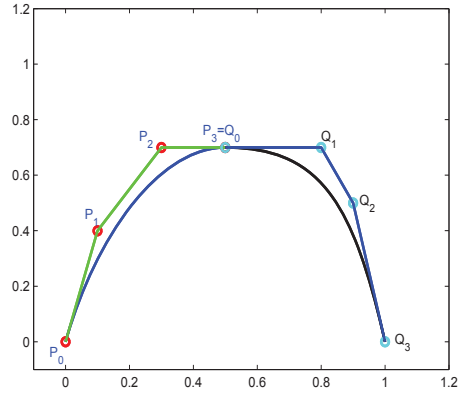
Let $P(\theta)$, $Q(\theta)$ be the two curve segments defined as $P(\theta) = \sum_{i=0}^3 P_i S_i(\theta)$ and $Q(\theta) = \sum_{i=0}^3 Q_i S_i(\theta)$ where P_i , Q_i with $i = 0, \dots, 3$ are control points of two curve segments and $S_i(\theta)$, $i = 0, \dots, 3$ are basis functions defined in Equation (3.1) with $0 \leq \theta \leq 1$.

The parametric continuity is defined as

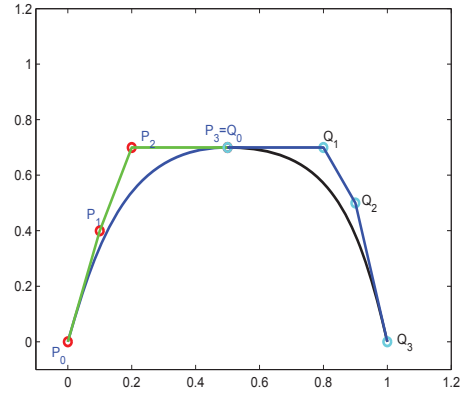
C^n continuity: derivatives (up to n^{th}) at the common end points are same

$$P^i(1) = Q^i(0) \quad i = 0, \dots, n. \quad (3.2)$$

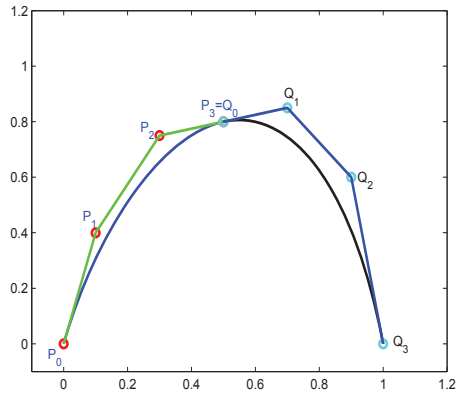
Figure 3.8 represents the parametric continuity between two curve segments.



(a) C^0 continuity $P(1) = Q(0)$



(b) C^1 continuity $P^i(1) = Q^i(0), i = 0, 1$



(c) C^2 continuity $P^i(1) = Q^i(0), i = 0, 1, 2$

Figure 3.8: Parametric continuity

The geometric continuity (GC) is defined as

$$GC^0 : \text{if } Q(0) = P(1)$$

$$GC^1 : \text{if } Q(0) = P(1), \text{ and}$$

$$Q'(0) = \lambda P'(1), \quad \lambda > 0.$$

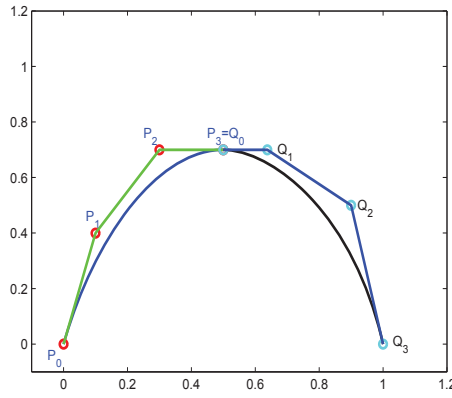
GC^2 : if $Q(0) = P(1)$, and

$Q'(0) = \lambda P'(1)$, and

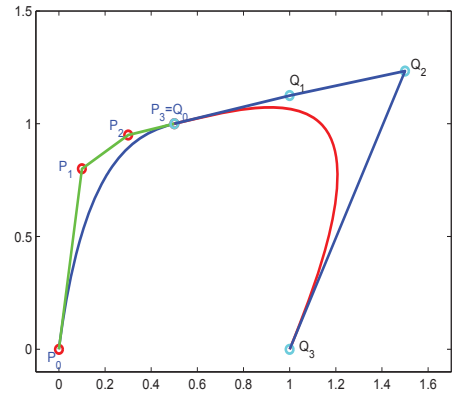
$Q''(0) = \lambda^2 P''(1) + \gamma P'(1)$,

where $\lambda > 0$, γ is an arbitrary value.

GC^1 continuity between two curves segments will be C^1 if we take $\lambda = 1$. Figure 3.9 represents geometric continuity between two curve segments.



(a) GC^1 continuity $\lambda = 1.3$



(b) GC^2 continuity $\lambda = 0.5, \gamma = 1.2$

Figure 3.9: Geometric continuity

3.2 The Rational Cubic Ball Curves

Rational cubic Ball curves with different conditions will be discussed in this section.